Science Advances
AAAS

advances.sciencemag.org/cgi/content/full/7/6/eabb7118/DC1

Supplementary Materials for

Denitrifying pathways dominate nitrous oxide emissions from managed grassland during drought and rewetting

E. Harris*, E. Diaz-Pines, E. Stoll, M. Schloter, S. Schulz, C. Duffner, K. Li, K. L. Moore, J. Ingrisch, D. Reinthaler, S. Zechmeister-Boltenstern, S. Glatzel, N. Brüggemann, M. Bahn

*Corresponding author. Email: eliza.harris@uibk.ac.at

Published 5 February 2021, *Sci. Adv.* **7**, eabb7118 (2021)
DOI: 10.1126/sciadv.abb7118

This PDF file includes:

1 Supplementary materials:

1.1 Trend in tropospheric N_2O mixing ratio

To examine the recent acceleration in the rate of increase of atmospheric N_2O mixing ratio, we used data from the two of longest running atmospheric background stations: Barrow Atmospheric Baseline Observatory (NOAA, HATS and CCGG flask sampling data; (*8*)) and Cape Grim Baseline Air Pollution Station (ALE/GAGE/AGAGE data; (*10, 101*)). The Barrow data from 1977 to 1995 was made with an older GC system and had an offset of 1.87 nmol mol^{-1} relative to the newer data, which was corrected before calculating growth rate. The growth rate calculated from this earlier data may be more uncertain, as indicated in Figure SS1. The AGAGE and NOAA datasets have a small offset (*10*), however this does not affect growth rate calculation at the individual stations. The atmospheric growth rate was calculated for 10 year blocks of data throughout the measurement period using the R function `lm` (*98*) (Figure SS1). The growth rate has increased from around 0.75 to 0.95-1.0 nmol mol^{-1} a^{-1}. We used the two-box model described in (*21*) to estimate the emission strength required to account for this acceleration, and find it corresponds to an increase of around 2 ± 0.4 Tg N_2O-N in annual anthropogenic emissions. This is equivalent to N_2O emissions of 0.036 ± 0.007 nmol m^{-2} s^{-1} for global ice-free land, or 0.24 ± 0.1 nmol m^{-2} s^{-1} for present-day agricultural land, using areas reported in (*7*).

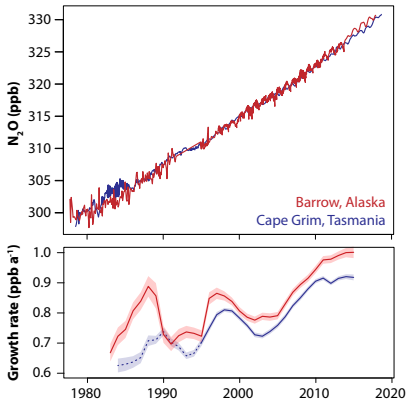

Figure S1: N_2O mixing ratio and growth rate for Barrow, Alaska and Cape Grim, Tasmania. Growth rate is calculated for 10-year blocks centred on the plotted date; uncertainty is shown as the shaded area. Barrow data and growth rate from before 1995 has increased uncertainty due to the older GC system, and growth rate for this period is thus indicated with a dotted line. Barrow data is attributed to the NOAA flask monitoring program (*8*) and Cape Grim data is from the AGAGE monitoring network (*10, 101, 102*).

1.2 Isotopic composition to distinguish N_2O production pathways

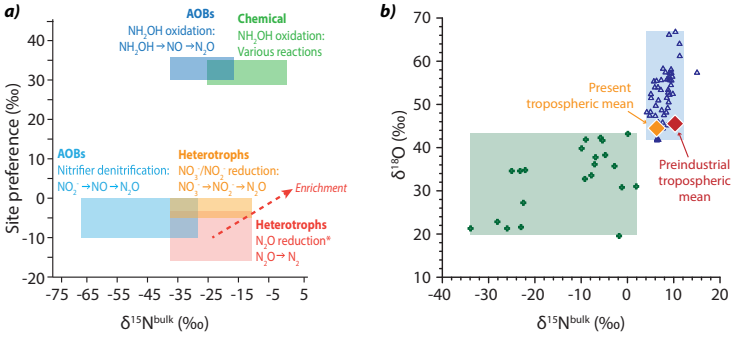

Figure S2: *a*) Microbial sources of N_2O, with isotopic signatures from (*42, 103–108*). *b*) Isotopic ranges for natural terrestrial (blue) and oceanic (green) sources of N_2O, compared to the preindustrial (*109*) and present-day average tropospheric isotopic composition (*78*).

1.3 Materials and methods: Supplementary information

1.3.1 Supplementary tables

Table S1: Summary of important dates throughout the experimental period. All times given refer to Central European Time (CET).

Date	Time	Action
07.05.18		Monoliths collected at Kaserstatt Alm
14.05.18		Monoliths transported from Kaserstatt Alm to Innsbruck
21.05.18		HOBO data loggers (SWC/T) and chamber collars installed on monoliths
22.05.18		LICOR flux measurements began
13.06.18		Full measurement system installed (Figure M1)
02.07.18	12:20	Fertilisation of monoliths in groups B/D, 200 kg N ha^{-1} as NH_4NO_3
05.07.18	12:15	Fertilisation of monoliths in groups A/C, 200 kg N ha^{-1} as NH_4NO_3
11.07.18	10:00	Rain out shelter erected
11.07.18	12:30	'Initial' soil sampling of all monoliths
30.08.18	11:30	'Pre-rewetting' soil and leachate sampling of monoliths in groups B and C
03.09.18	11:45	Rewetting of monoliths in groups B and C
06.09.18	10:30	'Post-rewetting' soil and leachate sampling of monoliths in groups B and C
06.09.18	10:30	'Pre-rewetting' soil and leachate sampling of monoliths in groups A and D
11.09.18	13:15	Rewetting of monoliths in groups A and D
13.09.18	07:30	'Post-rewetting' soil and leachate sampling of monoliths in groups A and D
18.09.18	09:45	Removed rain-out shelter
05.11.18		Final measurements made
12.11.18		All biomass in monoliths sampled down to the soil
19-20.11.18		Destructive 'final' soil sampling of monoliths in layers

Table S2: Isotopic composition of calibration gas types. [a]Mean isotopic composition and standard deviation over 5 months, measured using Picarro G5131i with N_2O mixing ratio of 330 nmol mol^{-1}, and calibrated with Cal1 and Cal2. [b] Known isotopic composition, measured by Empa/TiTech (J. Mohn, 2018, personal communication.

Abbreviation	$\delta^{15}N^{bulk}$ (‰)	SP (‰)
AmbFS [a]	5.3±1.6	17.0±4.5
AmbIso [a]	7.7±1.0	19.7±4.1
Comp [a]	4.8±1.7	14.3±6.1
MRDep [a]	0.9±2.8	1.9±8.6
Cal1 [b]	-47.35±0.18	-2.48±0.50
Cal2 [b]	6.85±0.06	20.54±0.24

1.3.2 Supplementary figures

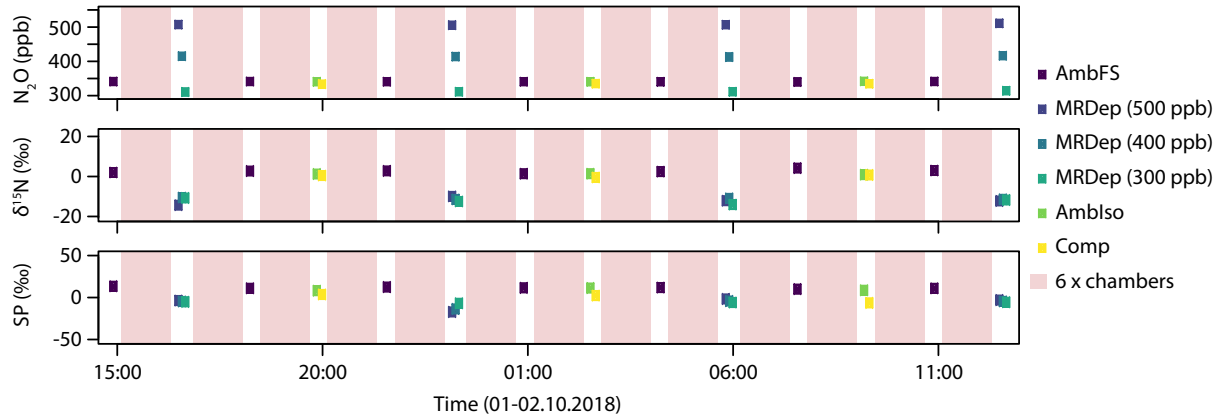

Figure S3: A typical measurement sequence including calibration and mixing ratio dependence measurements, as well as blocks of 6 chamber measurements. Isotope data in this figure is corrected for mixing ratio dependence but not calibrated.

1.3.3 Testing CPM using a simulated N_2O timeseries

CPM was tested with a simulation of N_2O fluxes and isotopic composition at 3-hour intervals across the measurement period. At each 3-hour timestep (t_i), the fraction of N_2O from denitrification was simulated according to:

$$f_{\mathrm{D},t_i} = f_{\mathrm{D},t_{i-1}} + 0.1 \times r \quad \text{where} \, 0 \leq f_{\mathrm{D}} \leq 1 \tag{7}$$

where r is a normally distributed random number with $\mu = 0$ and $\sigma = 1$, and $f_{\mathrm{N},t_i} = 1 - f_{\mathrm{D},t_i}$. The fraction of N_2O reduced (f_{R,t_i}) at each time step was determined the same way. The N_2O flux was set at 1 nmol m^{-2} s^{-1}, reduced by consumption according to f_{R,t_i}. 10% hourly variability is much higher than that observed for N_2O fluxes, which vary by 0.5-2% on average between each measurement for the different monoliths - thus this level of variability in simulated pathways will give a robust test of CPM.

The isotopic composition of the directly emitted N_2O was found from Eq. 5 (Methods) using end members of -10 and 30‰ and -5 and 0‰ for SP and δ^{15}N for denitrification and nitrification respectively. The absolute values of the δ^{15}N endmembers depend on substrate isotopic composition, thus these are approximations based on measurements showing δ^{15}N fractionation favours the light isotope more strongly during denitrification than nitrification (*86*). The measured SP and δ^{15}N of N_2O following reduction were calculated with Eq. 6 (Methods).

N_2O production and consumption pathways for the simulated data were calculated using CPM, and compared to the input (ie. true) production pathways, shown in red in Figure SS4. To investigate the sensitivity of results to the chosen isotopic parameters, the base isotope fractionation factors as well as tests with SP_D = 0‰, SP_N = 35‰, α_{SP} = -7.0‰ and $\alpha_{15N-bulk}$ = -9.3‰ were used to produce the simulated data - these values represent the observed ranges (SP_D, SP_N, (*86*)) or the best estimates for isotopic fractionation +1 standard deviation (*18*). The

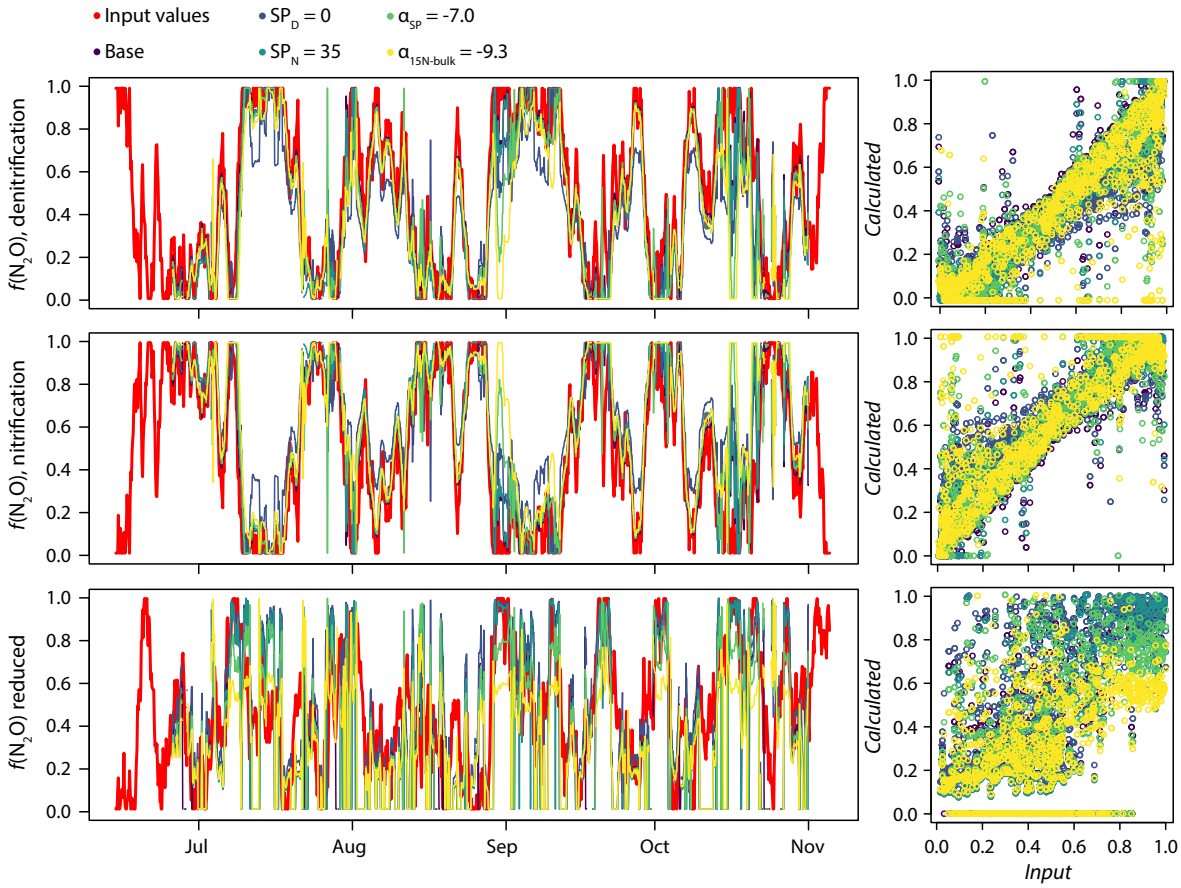

Figure S4: Comparison of input fractions of denitrification, nitrification and reduction (shown in red in the left panels and on the x-axis in the right panels) to fractions calculated using CPM with simulated isotopic data. The 'base' simulation uses best estimates for isotopic fractionation. The four additional simulations use varying input values for the different isotopic parameters.

base values were always used to calculate the pathways from the simulated data with CPM, thus this approximates the sensitivity of the approach to inaccurate fractionation factors.

CPM performed very well to distinguish between different production pathways, with an RMSE of 0.1, 0.1 and 0.27 for denitrification, nitrification and N_2O reduction respectively (Figure SS4). There was no mean difference between input and calculated partitioning for denitrification and nitrification. When reduction was high and strongly varying within the 12-hour window, there was often no correlation detected by CPM and thus reduction was calculated

to be 0 - therefore reduction is underestimated by 10% overall. In reality, reduction is not often expected to be both high (>80%) and strongly variable within a short 12-hour window. When the input isotopic fractionation factors were varied, the model still performed strongly, as it was robust to these changes: RMSE for denitrification and nitrification was worst (0.2) when $\alpha_{15N-bulk}$ = -9.3‰. RMSE is <0.28 for reduction for all tested isotope values shown in Figure SS4 - differences are only seen when reduction is >80%.

Given the satisfactory performance of CPM with simulated data, this method was adopted to partition N_2O production and consumption pathways for the measurement data presented in this paper. Over the entire measurement period, SP_{mean} was less than SP_D (100% denitrification) 57% of the time. $SP_N < SP_{mean} < SP_D$ but there was no evidence of reduction 31% of the time. There was evidence of reduction 12% of the time. The low overall level of reduction and low variability of N_2O fluxes on a 12-hour timescale is ideal for the CPM approach - more highly variable data with higher levels of reduction would require higher measurement frequency and thus smaller time windows to apply the CPM approach.

1.4 Extended results

1.4.1 Instrument performance

The chamber-spectrometer set up (Section 1.2, Methods) ran from June 15 to November 5 with few interruptions; gaps of more than 24 hours in isotope data are present only from 6-10 September and 5-17 October due to the instrument computer crashing. The measured isotope data was significantly dependent on mixing ratio throughout the experiment (Figure SS5a). The dependence on mixing ratio changed over time, showing the importance of regular calibration with gases at varying mixing ratios. This may introduce extra uncertainty into the results from before July 31, when the full calibration set up was installed. No other dependencies on mixing ratios or laser parameters were observable within the ranges seen in the normal running chamber

set up.

Following correction for mixing ratio dependence and drift (Section 1.2.3, Methods), the final data for each calibration gas type showed a standard deviation of 1-3, 4-9 and 30-45‰ for δ^{15}N, SP and δ^{18}O respectively (Table SS2), which compares very well to previous studies (*40, 110*). An example of the data quality over 5 months is shown in Figure SS5b as histograms of all measurements of AmbFS. The instrumental set up showed very good performance for δ^{15}N and satisfactory performance for SP, however for δ^{18}O the data quality was extremely poor and the data could not be used. No specific relationship could be found between δ^{18}O and any other parameter measured in the system, pointing towards an unknown interference causing the noisy data.

The most critical point regarding instrumental performance is the final uncertainty in calculated source isotopic composition for N_2O emission (or consumption), as measured using chambers. The resultant error in source isotopic composition relative to N_2O flux is shown in Figure SS5c. The results are similar for δ^{15}N and SP, with uncertainty in source isotopic composition steeply decreasing as fluxes increase to around 1 nmol m^{-2} $s-1$ and then reaching a plateau. To apply this method for lower fluxes, for example in winter or at extensively managed or unfertilised sites, it would be necessary to either increase chamber closure times to longer than 15 minutes or improve the chamber surface area-to-volume ratio, or alternatively perform preconcentration of N_2O from the chamber before measuring isotopic composition (*40*). Instrumental improvements allowing the Picarro 5131i to operate in recirculation mode and thus removing the need for the small (30 sccm) dilution with ambient air will also facilitate isotopic measurements for low flux sites.

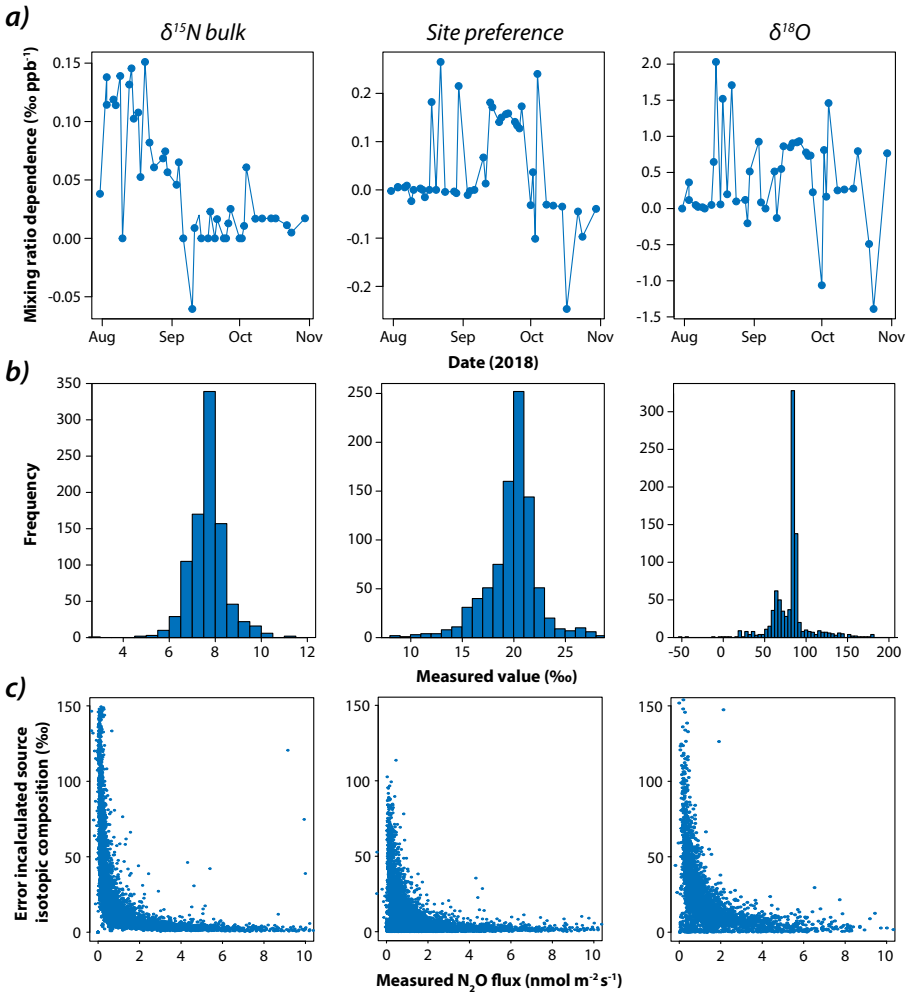

Figure S5: A summary of the isotope data quality over the 5-month measurement period. From left to right the panels show δ^{15}N, SP and δ^{18}O respectively. The top row of the figure (a) shows the calculated mixing ratio dependence for each 1-5 day block; all points are significant at $p < 0.05$. The middle row (b) shows histograms of all AmbFS measurements. The bottom row (c) shows the relationship between N_2O flux magnitude and error in calculated source isotopic composition using a Keeling plot approach on measured chamber data for a 15 minute closure time.

1.4.2 Strength of the drought treatment

For this study, drought is defined as a complete absence of precipitation, which subsequently leads to stress and thus reduced biomass growth (*77*) (Figure SS6). The average precipitation for July and August from 1858-2018 is 242±62 mm, and the average precipitation amounts for the exact drought periods (11.07.2018 to 03.09.18 (D1) or 11.09.2018 (D2)) are 253±80 mm and 275±78 mm respectively for 2015-2018 (Figure SS6). The maximum timespan with <1 mm of precipitation per day in summer (June-September) for 2015-2018 is 16 days in 2018, compared to around 8 weeks in this study. The drought applied in this study is therefore clearly extreme - around four standard deviations below the mean precipitation and around four times longer than the longest recent summer drought. This data is for Innsbruck University weather station, which is the longest running precipitation dataset close to the measurement site. Longterm monthly data is from the ZAMG HISTALP project (Historical Instrumental Climatological Surface Time Series Of The Greater Alpine Region; http://www.zamg.ac.at/histalp/); 10-minute data from 2015-2018 is from the TAWES (Teilautomatische Wetterstation) station operated jointly by the ZAMG and the University of Innsbruck.

WFPS steadily decreased throughout the drought treatment until the rewetting on day 54 and 62 for D1 and D2 respectively (Figure SS8). The measured permanent wilting point (pF = 4.2; see Methods, Section 4.3) for these soils is around 19±6% WFPS, which was reached between day 19 and 50 for each of the seven D monoliths (mean = day 36). This was clearly reflected in plant growth (dry mass), which was significantly reduced for drought monoliths compared to control from the third week of the drought ($p < 0.05$; Figure SS6). The final assessment of biomass composition showed that D monoliths had significantly less dry forb biomass than C and W monoliths but the same dry grass biomass, for both dead and live grasses and forbs. In particular, D monoliths had no forbs from the genus *Geum*, while *Geum sp.* made up 12% and 15% of C and W forb biomass respectively.

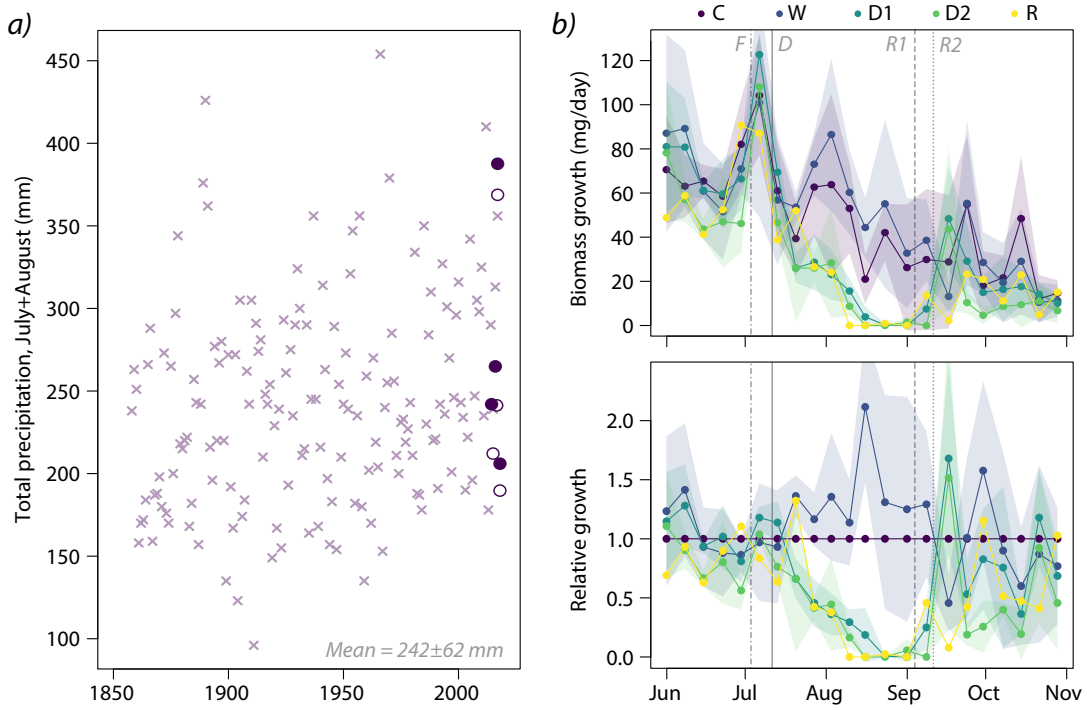

Figure S6: Strength of the drought treatment: *a)* Mean precipitation for July and August from 1858 to 2018 from the weather station at Innsbruck University, 18 km from the Kaserstatt Alm, using monthly data is from the ZAMG HISTALP project (Historical Instrumental Climatological Surface Time Series Of The Greater Alpine Region; http://www.zamg.ac.at/histalp/). The precipitation corresponding to the exact drought time periods for 2015-18 are shown with the open circle indicating D1 and the filled circle for D2 for each year, calculated using 10-minute data from the TAWES (Teilautomatische Wetterstation) station operated jointly by the ZAMG and the University of Innsbruck. *b)* Effect of drought treatment on biomass production. Shown in purple, blue and dark/light green is the mean value for C, W and D1/D2 monoliths; the shaded area shows the 1σ standard deviation. The R monolith is shown in yellow. The upper panel shows absolute growth (mg dry mass per day) and the lower panel shows growth relative to the control group. Times for fertilisation (F), drought start (D) and rewetting (R1/R2) are indicated.

1.4.3 NanoSIMS measurements

NanoSIMS measurements revealed significant differences in soil microaggregate (μm-range soil grains, (*96*)) chemical composition throughout the experiment (Table SS3 and Figure 3). Average grain size increased throughout the experiment for the control treatment; however this effect was not seen for the drought treatment, which had smaller average grain size than controls at peak drought. This may reflect organic matter production binding grains, which was slowed by the drought (*47*). No significant differences in ion count rates or ratios were seen between control grains at any point in time, nor between control and drought treatments at initial and post-rewetting timesteps (Table SS3).

Count rates reflect not only elemental concentration, but also chemistry and topography of the sample - thus, they can indicate changes in particles although caution should be taken extrapolating count rate differences directly to elemental differences. Ratios provide a more robust comparison between samples. Count rates for the drought treatment at peak drought were significantly higher than the control for $^{12}C^-$, $^{12}C_2^-$, $^{12}C^{14}N^-$ and $^{32}S^-$ as well as ratios $\frac{^{12}C^{14}N^-}{^{16}O^-}$ and $\frac{^{14}N^{16}O_2^-}{^{16}O^-}$. These count rates and ratios were also all significantly higher for the drought treatment at peak drought compared to initial and/or rewetting time periods. These consistent trends indicates an actual difference in composition at peak drought, despite the difficulties in interpreting count rates. Most of these ions and ratios can be taken as representative of the distribution of soil organic matter and nitrogen-bearing organic matter (N-SOM) (*47, 48*). Sulfur-containing material clearly showed the same drought-dependent reversible enrichment, which may indicate the source of the changes is microbial death, subsequently releasing organic components including S- and N-containing amino acids and other biomolecules (*56*). Some differences were also evident for the $^{14}N^{16}O_2^-$ ion. However, nitrite is extremely soluble and may have been affected by the sample preparation; it is also unstable in the high vacuum conditions of the NanoSIMS, therefore these changes cannot be accurately interpreted (*48*).

In summary, the observed changes in secondary ion count rates and ratios reflect a reversible enrichment in S- and N-SOM, without a consequent enrichment in oxygen at the surface of soil grains subjected to drought (Figure 3). This was not evident in the measurements of bulk soil C and N (data not shown), which show no differences between treatment or time period through the experiment.

Table S3: NanoSIMS measurement results comparing control and drought treatments at initial (I), peak drought (D) and post-rewetting (R) time periods. n (monoliths) refers to the number of monoliths studied at each timestep while n (grains) refers to the number of individual grains measured in the NanoSIMS. Size is the average grain size. In the lower part of the table, count rates (counts s^{-1}) are given for the 7 secondary ions and 3 ratios indicated. The standard error for each value is shown, and significant differences are indicated: i) significant differences between treatments at the same time step, eg. control vs. drought at peak drought, are shown in bold, and ii) significant differences within a treatment at different times are indicated in the second line for each ion, eg. for $^{12}C^-$ control treatments show no changes whereas drought - peak drought (D) is different to initial (I) and post-rewetting (R). *$\times$1000 as count rates very low.

Treatment	Control	Control	Control	Drought	Drought	Drought
Period	Initial	Peak drought	Post-rewetting	Initial	Peak drought	Post-rewetting
n (monoliths)	1	4	1	1	4	1
n (grains)	17	30	22	20	77	40
Size (μm^2)	4±5	**10±17**	13±20	4±4	**6±9**	4±4
	D	I	-	-	-	-
$^{12}C^-$	5.5±1.4	**1.0±0.2**	0.2±0.2	0.05±0.02	**5.2±1.2**	0.2±0.2
	-	-	-	D	I,R	D
$^{16}O^-$	11.1±2.6	18.3±6.1	22.8±3.5	15.5±3.3	15.0±2.0	17.1±1.6
	-	-	-	-	-	-
$^{12}C_2^-$	10.1±2.1	**2.8±0.6**	3.7±0..3	3.1±0.5	**14.3±2.8**	1.9±0.6
	-	-	-	D	I,R	D
$^{12}C^{14}N^-$	5.6±1.0	**3.5±0.5**	7.7±0.7	2.9±0.6	**10.3±1.7**	2.3±0.5
	-	-	-	D	I,R	D
$^{28}Si^-$	8.9±2.9	3.3±0.8	2.7±0.8	2.1±0.6	3.9±1.1	1.3±0.5
	-	-	-	-	-	-
$^{32}S^-$	0.4±0.1	**0.5±0.1**	0.9±0.1	0.8±0.2	**4.8±1.3**	0.5±0.1
	-	-	-	-	R	D
$^{14}N^{16}O_2^-$ *	2.2±0.6	0.6±0.1	7.8±2.5	214±110	258±74	0.8±0.2
	-	-	-	-	R	D
$\frac{^{12}C^{14}N^-}{^{16}O^-}$	1.1±0.1	**0.7±0.1**	0.7±0.1	0.3±0.1	**1.7±0.2**	0.3±0.1
	-	-	-	D	I,R	D
$\frac{^{14}N^{16}O_2^-}{^{16}O^-}$ *	0.2±0.03	**0.1±0.03**	0.2±0.05	7.5±3.6	**10.2±2.7**	0.1±0.02
	-	-	-	-	R	D
$\frac{^{14}N^{16}O_2^-}{^{12}C^{14}N^-}$ *	0.4±0.1	0.2±0.04	1.6±0.7	59±32	25±11	0.3±0.08
	-	-	-	-	-	-

1.4.4 Watering of the control and wet monoliths

N_2O fluxes and isotopic composition were monitored for at least 24 hours after regular watering of the non-drought monoliths, which occured 55 and 57 times for control and wet treatments respectively. Each watering event increased the WFPS by 1.9 and 1.7% for control (C) and wet (W) respectively (Figure SS7), with peak WFPS occurring approximately 12 hours after watering and decreasing thereafter. Two days after watering WFPS had returned to the initial level. CPM could only be applied to the mean for all monoliths as data quantity was insufficient for individual watering events. Average N_2O fluxes peaked due to denitrification 1-2 days after watering for C monoliths, and showed a minor peak 0.5-1 days after watering for W monoliths (Figure SS7). The only significant change in pathways linked directly to watering was an increase in denitrification for C monoliths immediately after watering.

When each watering event was considered individually, the WFPS before watering and the WFPS change with watering showed a significant negative correlation ($p < 0.05$, data not shown) - at higher WFPS, monoliths were able to take up less water, so WFPS increased less with watering - thus WFPS increased less for average watering of W monoliths. 54% of variability in N_2O changes could be explained by the WFPS before watering: When WFPS was higher, the increase in N_2O flux with watering was larger ($p < 0.01$). There was a great deal of variability in the response of N_2O emissions to watering, with fluxes 12 hours before and after watering changing by -1.2 to +2.5 nmol m^{-2} s^{-1} for C and -0.2 to 6.9 nmol m^{-2} s^{-1} for W monoliths. The differences between baseline emissions, outside of watering peaks, between C and W monoliths was much larger than changes induced immediately after watering, and are discussed in the main article.

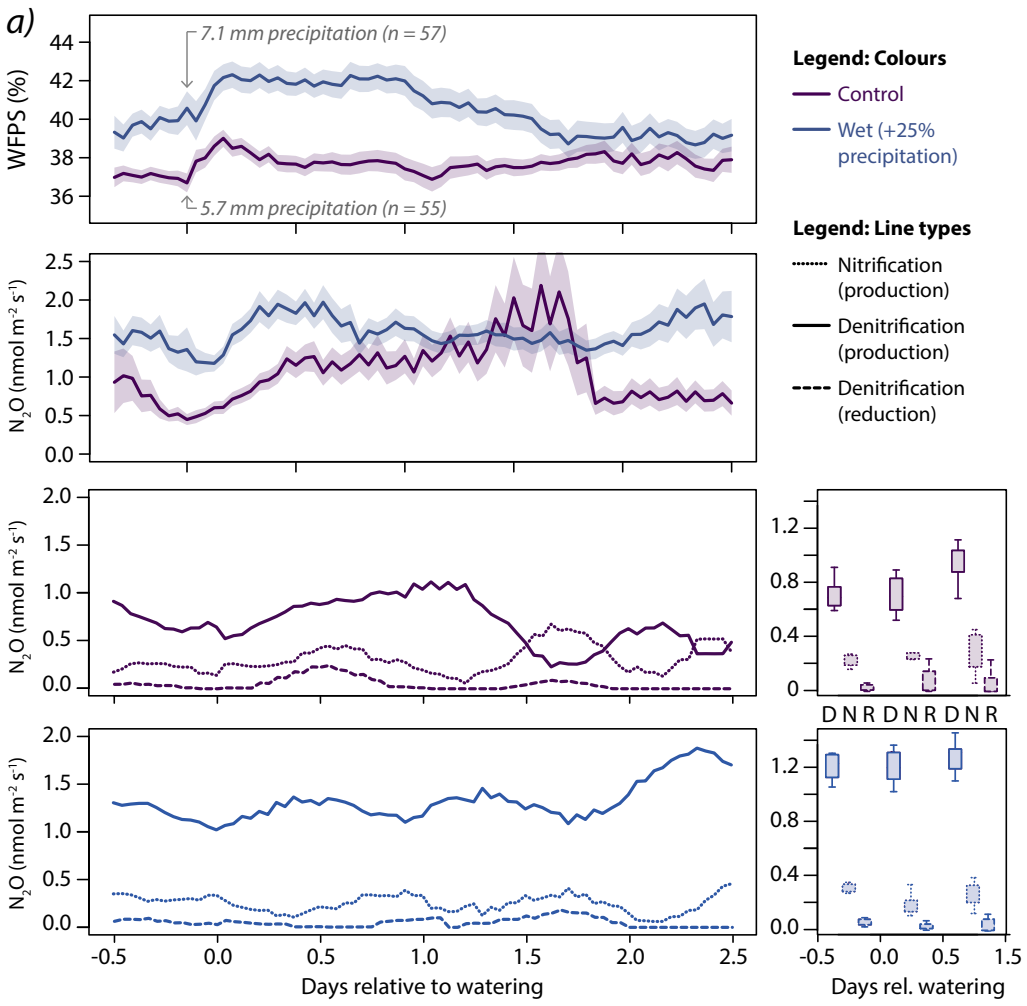

Figure S7: Effect of watering on N_2O emissions from control and wet monoliths. The top two panels show WFPS and N_2O flux with the standard error shown as the shaded area ($n = 4$ for C/W). The bottom panels show N_2O flux via different pathways as a time series on the left and as a mean for different time periods on the right.

1.4.5 Additional figures and tables

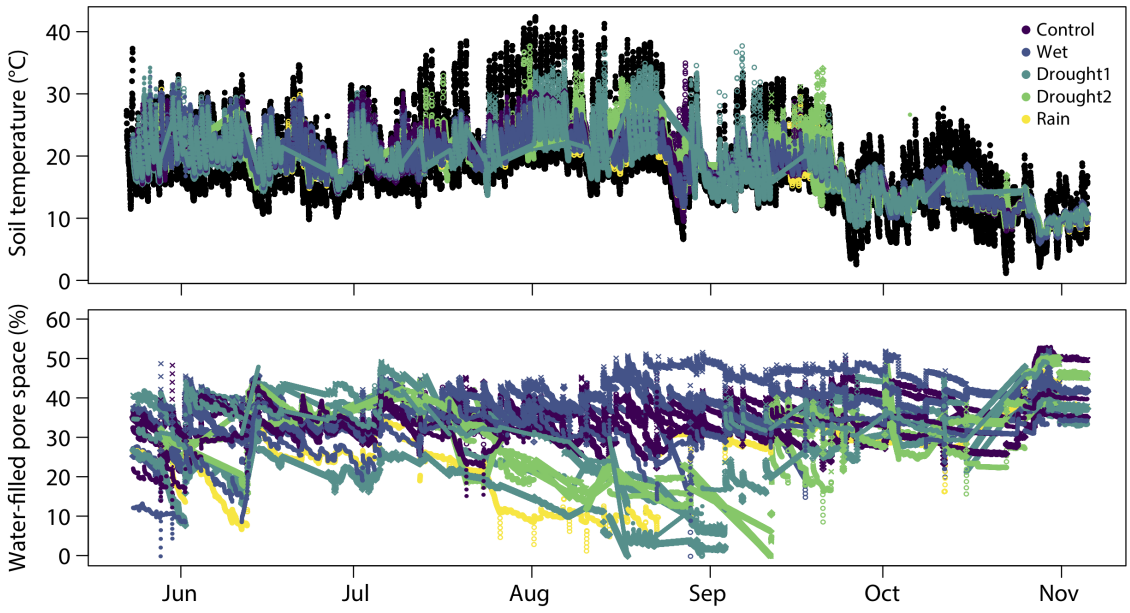

Figure S8: Soil temperature (upper panel) and water-filled pore space (lower panel) for the 16 monoliths for the entire experimental period. The surface air temperature is shown in black for comparison.

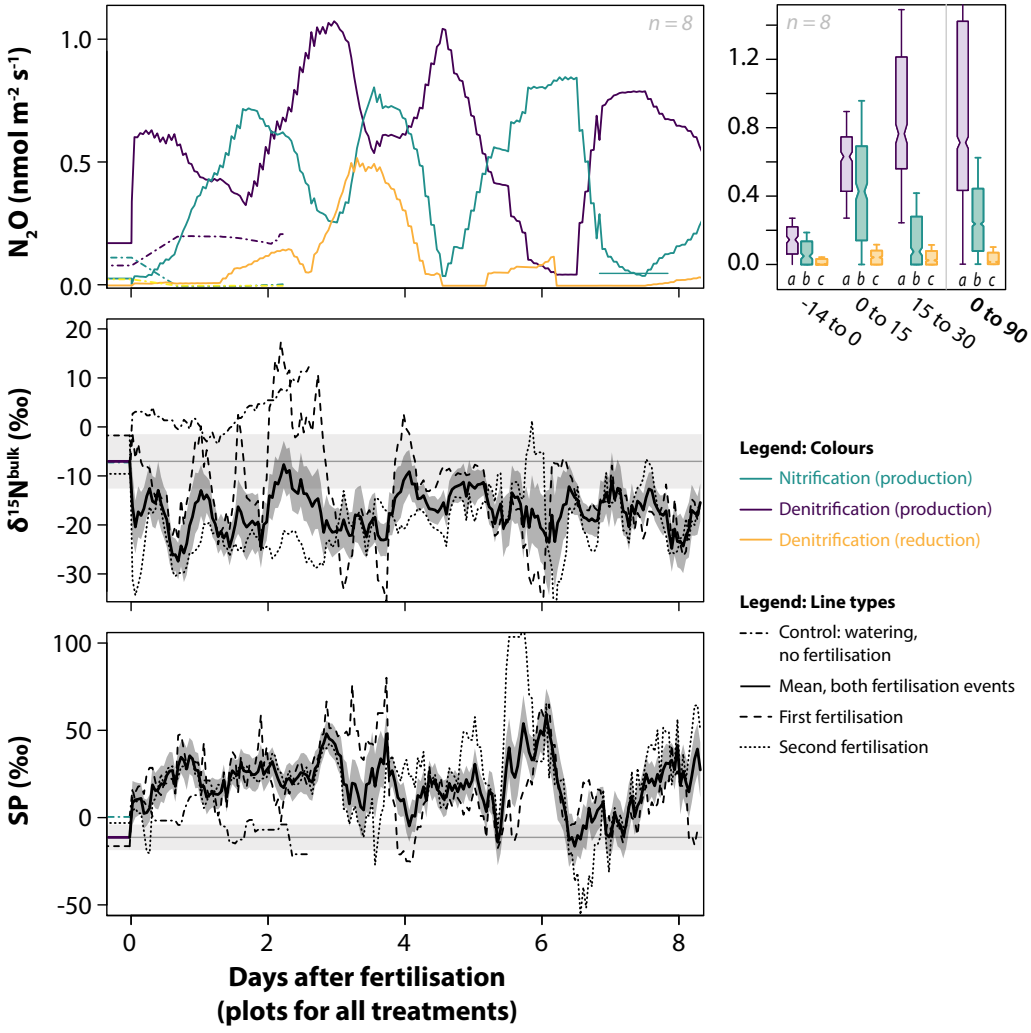

Figure S9: Effect of fertilisation on N_2O production and consumption via different microbial pathways, as well as measured isotopic composition, indicated using different line colours as shown in the legend. Line types show the first and second fertilisation events, the mean, and the control as indicated. The mean for the four days before fertilisation is shown at the beginning of each time series as a baseline. At the right hand side, box plots compare the pathways over a longer time period - this only uses data from non-drought plots, as the drought treatment began 10 days after the first fertilisation. Letters below the box plots indicate significant differences between treatments at each time step.

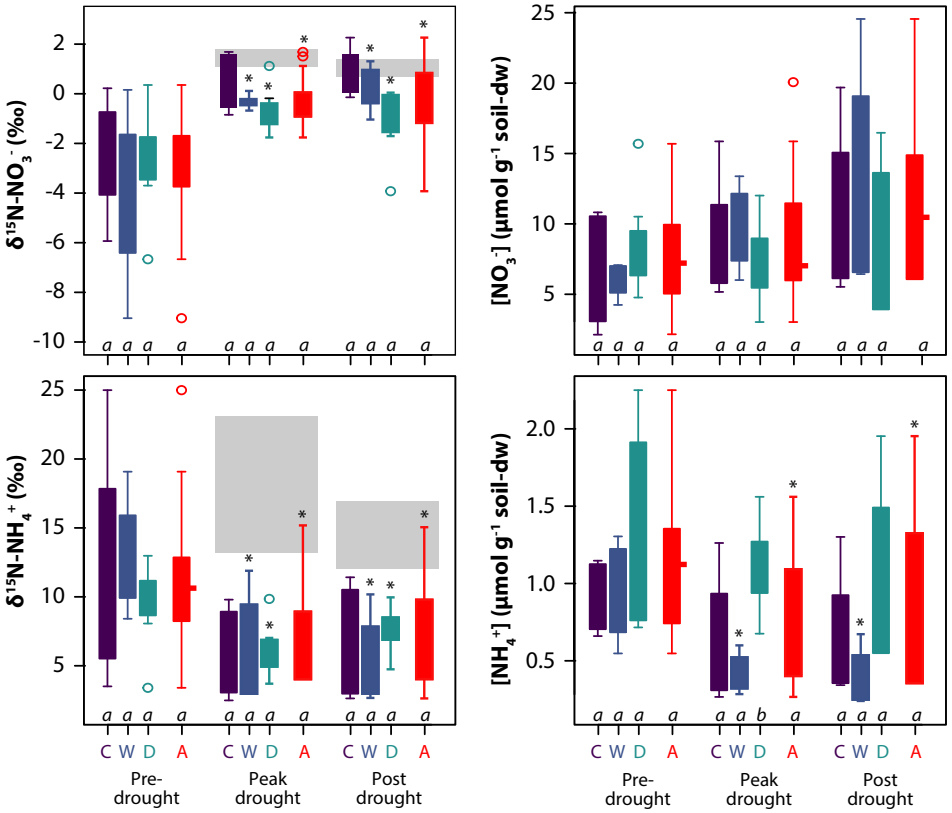

Figure S10: Isotopic composition and concentration of soil nitrate and ammonium before the beginning of a drought ('pre-drought', several days after fertilisation), at 'peak drought', and 2-3 days after rewetting ('post-drought'). The treatments are shown in purple, blue and green for C, W and D (D1 and D2) respectively ($n = 4, 4, 7$ respectively), with combined data for all monoliths shown in red ($n = 15$). Letters below the box plots indicate significant differences between treatments at each time step, while asterisks where present indicate significant differences between time steps for a particular treatment. Grey boxes indicated the mean isotopic composition of leached NO_3^- or NH_4^+ for a particular time period.

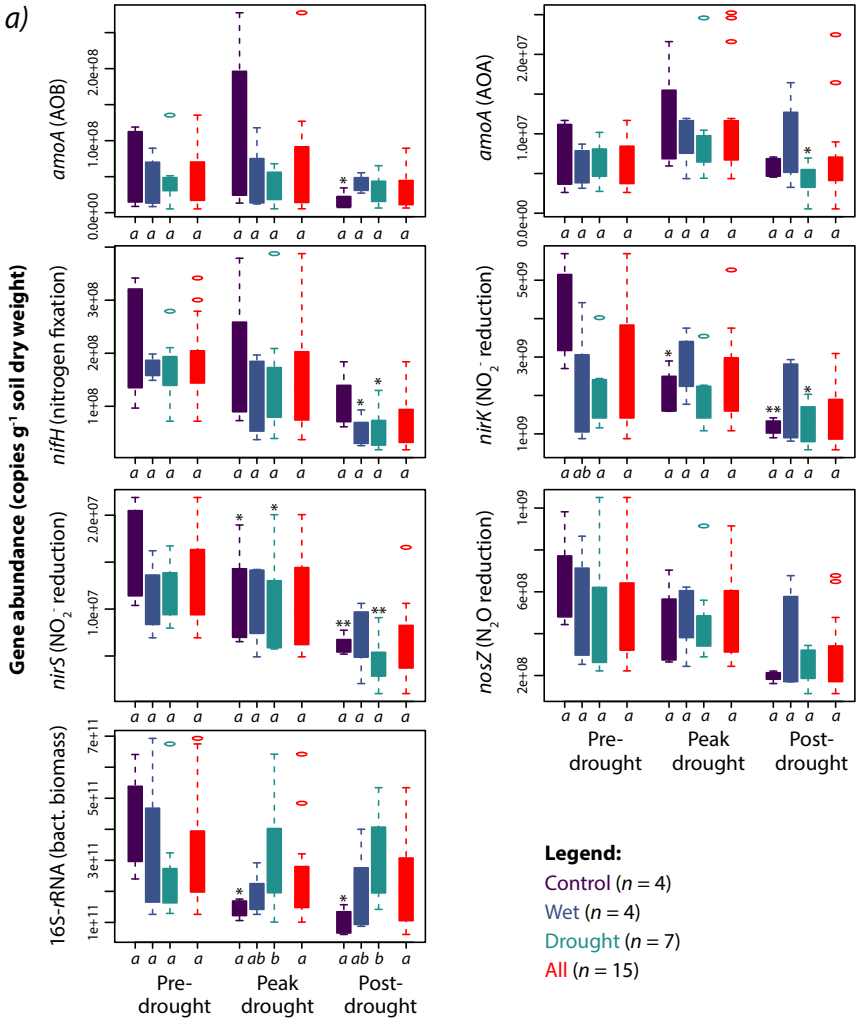
a)
Gene abundance (copies g-1 soil dry weight)
amoA (AOB)
amoA (AOA)
nifH (nitrogen fixation)
nirK (NO2- reduction)
nirS (NO2- reduction)
nosZ (N2O reduction)
16S-rRNA (bact. biomass)
Pre-drought
Peak drought
Post-drought
Legend:
Control (n = 4)
Wet (n = 4)
Drought (n = 7)
All (n = 15)

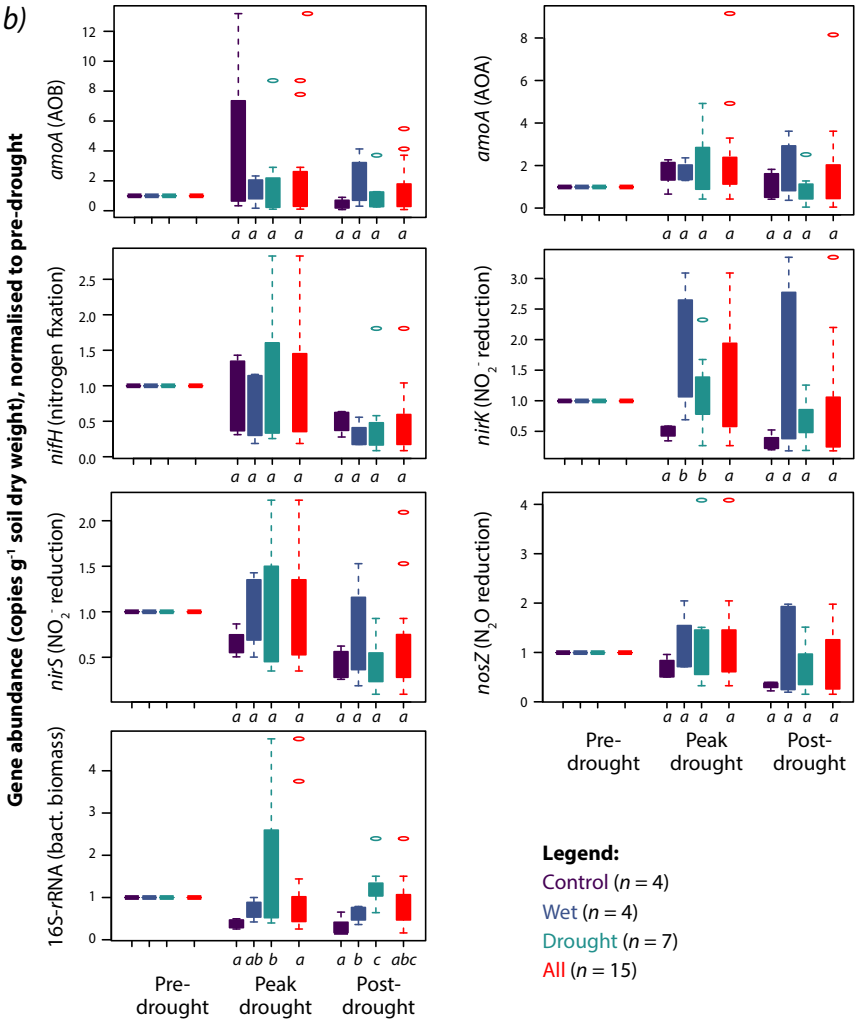

Figure S11: Microbial gene abundances measured for monolith soils with qPCR before the drought ('pre-drought', several days after fertilisation), at 'peak drought', and 2-3 days after rewetting ('post-drought'): Absolute values are shown in part a), whereas part b) shows results normalised to pre-drought. Letters below the box plots indicate significant differences between treatments at each time step, while asterisks where present indicate significant differences between time steps for a particular treatment.

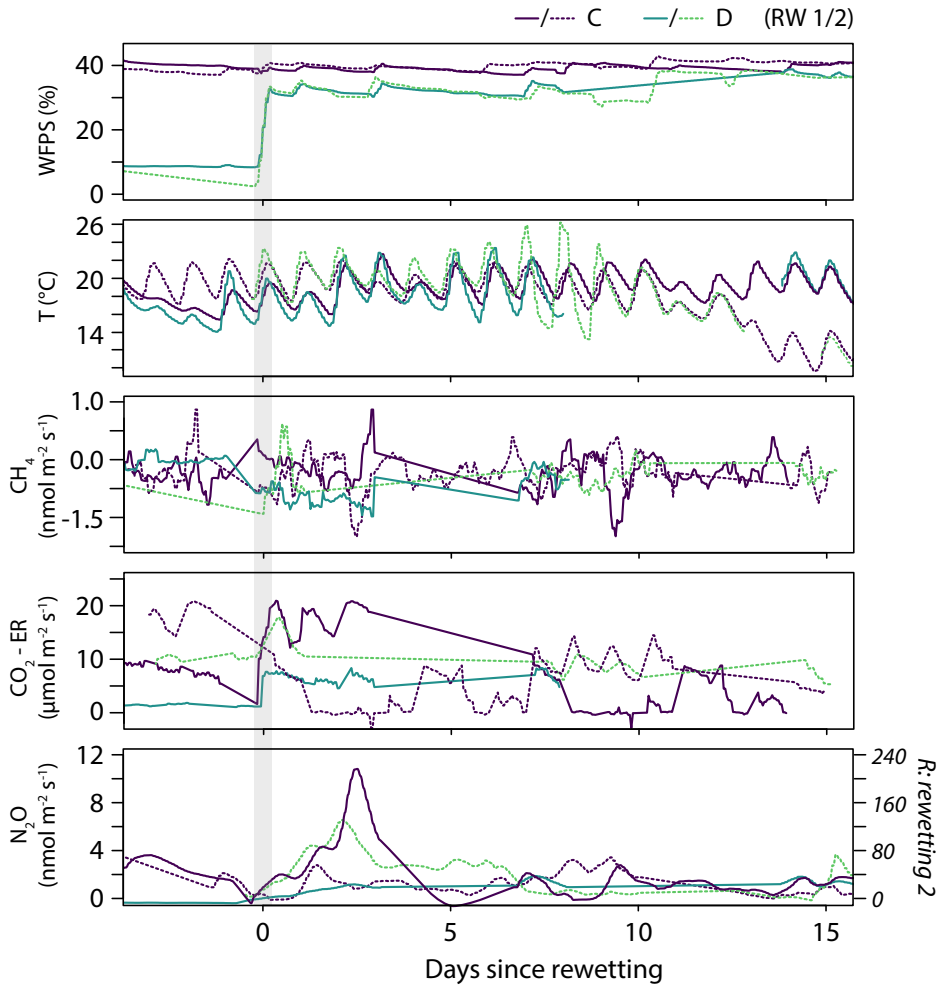

Figure S12: WFPS, temperature, CH_4 and CO_2 and N_2O fluxes following rewetting of the drought monoliths. CO_2 data is only ecosystem respiration (ER) - measurements with clear chambers are not included. C (control, n=4), D (drought, N=4/3) treatments are shown for the two rewetting events on 03.09 and 11.09.18 (shown as solid and dotted lines respectively.

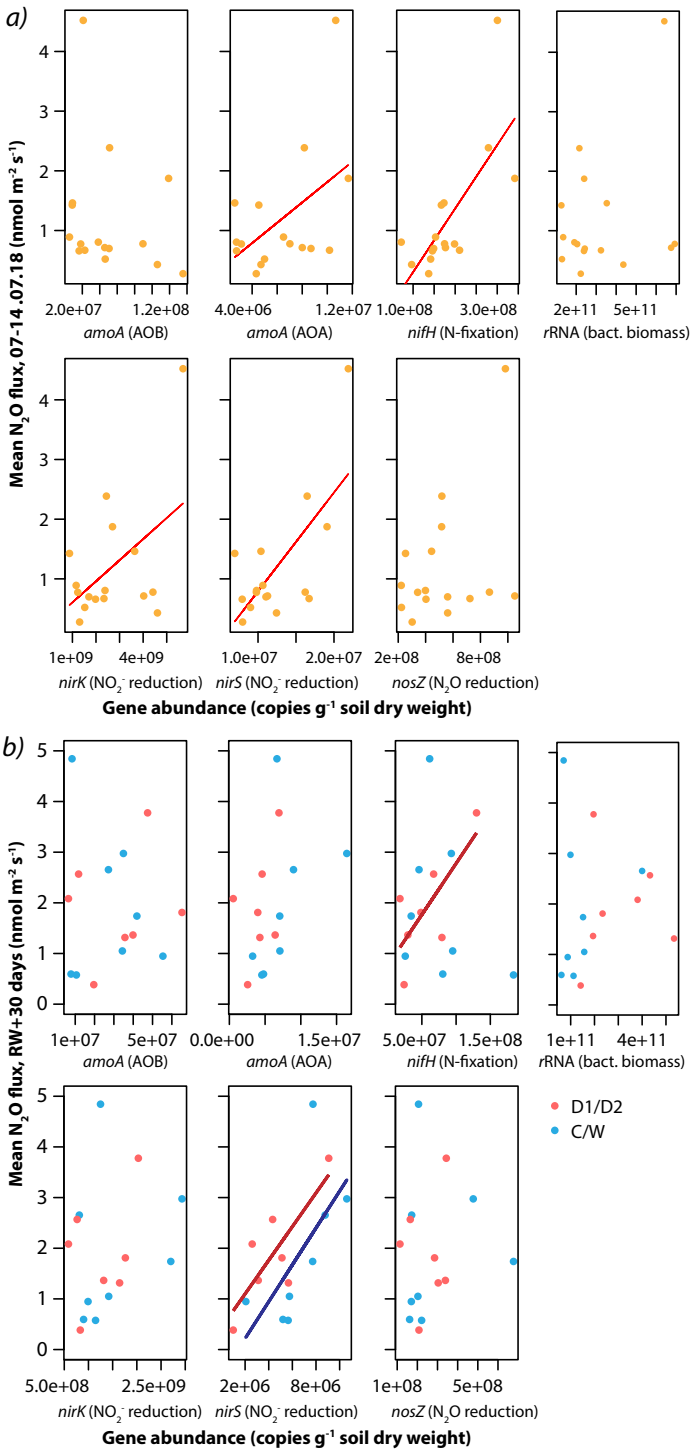

Figure S13: Relationship between microbial activity (microbial gene abundances measured with qPCR) and N_2O fluxes. *a)* Microbial gene abundances measured for all monoliths using soils collected on 12.07.18 plotted against mean N_2O fluxes before the drought (07-14.07.18). Significant linear regressions ($p < 0.05$) are shown in red. *b)* Microbial gene abundances measured for all monoliths using soils collected several days after rewetting (see Methods, Table SS1) plotted against mean N_2O fluxes for the 30 days after rewetting; drought treatment monoliths are shown in red and watered monoliths in blue.

REFERENCES AND NOTES

1. A. R. Ravishankara, J. S. Daniel, R. W. Portmann, Nitrous oxide (N_2O): The dominant ozone-depleting substance emitted in the 21st century. *Science* **326**, 123–125 (2009).
2. S. A. Montzka, E. J. Dlugokencky, J. H. Butler, Non-CO_2 greenhouse gases and climate change. *Nature* **476**, 43–50 (2011).
3. IPCC, *Climate Change 2014: Synthesis Report. Contribution of Working Groups I, II and III to the Fifth Assessment Report of the Intergovernmental Panel on Climate Change* (IPCC, 2014).
4. E. A. Davidson, The contribution of manure and fertilizer nitrogen to atmospheric nitrous oxide since 1860. *Nat. Geosci.* **2**, 659–662 (2009).
5. S. Park, P. Croteau, K. A. Boering, D. M. Etheridge, D. Ferretti, P. J. Fraser, K-R. Kim, P. B. Krummel, R. L. Langenfelds, T. D. van Ommen, L. P. Steele, C. M. Trudinger, Trends and seasonal cycles in the isotopic composition of nitrous oxide since 1940. *Nat. Geosci.* **5**, 261–265 (2012).
6. World Bank, *World Development Indicators: Fertiliser Consumption (AG.CON.FERT.ZS)* (World Bank, 2019).
7. H. Tian, J. Yang, R. Xu, C. Lu, J. G. Canadell, E. A. Davidson, R. B. Jackson, A. Arneth, J. Chang, P. Ciais, S. Gerber, A. Ito, F. Joos, S. Lienert, P. Messina, S. Olin, S. Pan, C. Peng, E. Saikawa, R. L. Thompson, N. Vuichard, W. Winiwarter, S. Zaehle, B. Zhang, Global soil nitrous oxide emissions since the preindustrial era estimated by an ensemble of terrestrial biosphere models: Magnitude, attribution, and uncertainty. *Glob. Chang. Biol.* **25**, 640–659 (2019).
8. E. J. Dlugokencky (2019); NOAA/GML (www.esrl.noaa.gov/gmd/ccgg/trends_n2o/).
9. R. L. Thompson, L. Lassaletta, P. K. Patra, C. Wilson, K. C. Wells, A. Gressent, E. N. Koffi, M. P. Chipperfield, W. Winiwarter, E. A. Davidson, H. Tian, J. G. Canadell, Acceleration of global N_2O emissions seen from two decades of atmospheric inversion. *Nat. Clim. Change* **9**, 993–998 (2019).
10. R. G. Prinn, R. F. Weiss, J. Arduini, T. Arnold, H. L. De Witt, P. J. Fraser, A. L. Ganesan, J. Gasore, C. M. Harth, O. Hermansen, J. Kim, P. B. Krummel, S. Li, Z. M. Loh, C. R. Lunder, M. Maione, A. J. Manning, B. R. Miller, B. Mitrevski, J. Mühle, S. O'Doherty, S. Park, S. Reimann, M. Rigby, T. Saito, P. K. Salameh, R. Schmidt, P. G. Simmonds, L. P. Steele, M. K. Vollmer, R. H. Wang, B. Yao, Y. Yokouchi, D. Young, L. Zhou, History of chemically and radiatively important atmospheric gases from the Advanced Global Atmospheric Gases Experiment (AGAGE). *Earth Sys. Sci. Data* **10**, 985–1018 (2018).
11. T. J. Griffis, Z. Chen, J. M. Baker, J. D. Wood, D. B. Millet, X. Lee, R. T. Venterea, P. A. Turner,

Nitrous oxide emissions are enhanced in a warmer and wetter world. *Proc. Natl. Acad. Sci. U.S.A.* **114**, 12081–12085 (2017).

12. F. Ehrhardt, J.-F. Soussana, G. Bellocchi, P. Grace, R. M. Auliffe, S. Recous, R. Sándor, P. Smith, V. Snow, M. de Antoni Migliorati, B. Basso, A. Bhatia, L. Brilli, J. Doltra, C. D. Dorich, L. Doro, N. Fitton, S. J. Giacomini, B. Grant, M. T. Harrison, S. K. Jones, M. U. F. Kirschbaum, K. Klumpp, P. Laville, J. Léonard, M. Liebig, M. Lieffering, R. Martin, R. S. Massad, E. Meier, L. Merbold, A. D. Moore, V. Myrgiotis, P. Newton, E. Pattey, S. Rolinski, J. Sharp, W. N. Smith, L. Wu, Q. Zhang, Assessing uncertainties in crop and pasture ensemble model simulations of productivity and N_2O emissions. *Glob. Chang. Biol.* **24**, e603–e616 (2018).
13. K. Butterbach-Bahl, E. M. Baggs, M. Dannenmann, R. Kiese, S. Zechmeister-Boltenstern, Nitrous oxide emissions from soils: How well do we understand the processes and their controls? *Philos. Trans. R. Soc. B* **368**, 20130122 (2013).
14. N. Wrage, G. L. Velthof, M. L. V. Beusichem, O. Oenema, Role of nitrifier denitrification in the production of nitrous oxide. *Soil Biol. Biogeochem.* **123**, A3–A16 (2018).
15. O. Spott, R. Russow, C. F. Stange, Formation of hybrid N_2O and hybrid N_2 due to codenitrification: First review of a barely considered process of microbially mediated N-nitrosation. *Soil Biol. Biochem.* **43**, 1995–2011 (2011).
16. T. J. Clough, G. J. Lanigan, C. A. M. de Klein, S. Samad, S. E. Morales, D. Rex, L. R. Bakken, C. Johns, L. M. Condron, J. Grant, K. G. Richards, Influence of soil moisture on codenitrification fluxes from a urea-affected pasture soil. *Sci. Rep.* **7**, 2185 (2017).
17. J. Wei, M. Zhou, H. Vereecken, N. Brüggemann, Large variability in CO_2 and N_2O emissions and in ^{15}N site preference of N_2O from reactions of nitrite with lignin and its derivatives at different pH. *Rapid Commun. Mass Spectrom.* **31**, 1333–1343 (2017).
18. D. Lewicka-Szczebak, J. Augustin, A. Giesemann, R. Well, Quantifying N_2O reduction to N_2 based on N_2O isotopocules-validation with independent methods (helium incubation and ^{15}N gas flux method). *Biogeosciences* **14**, 711–732 (2017).
19. D. Wu, R. Well, L. M. Cárdenas, R. Fuß, D. Lewicka-Szczebak, J. R. Köster, N. Brüggemann, R. Bol, Quantifying N_2O reduction to N_2 during denitrification in soils via isotopic mapping approach: Model evaluation and uncertainty analysis. *Environ. Res.* **179**, 108806 (2019).
20. E. Bai, B. Z. Houlton, Y. P. Wang, Isotopic identification of nitrogen hotspots across natural terrestrial ecosystems. *Biogeosciences* **9**, 3287–3304 (2012).

21. L. Yu, E. Harris, S. Henne, S. Eggleston, M. Steinbacher, L. Emmenegger, C. Zellweger, J. Mohn, Atmospheric nitrous oxide isotopes observed at the high-altitude research station Jungfraujoch, Switzerland. *Atmos. Chem. Phys.* **20**, 6495–6519 (2020).
22. A. Dai, Increasing drought under global warming in observations and models. *Nat. Clim. Change* **3**, 52–58 (2013).
23. A. Dai, T. Zhao, Uncertainties in historical changes and future projections of drought. Part I: Estimates of historical drought changes. *Clim. Change* **144**, 519–533 (2017).
24. T. Zhao, A. Dai, Uncertainties in historical changes and future projections of drought. Part II: Model-simulated historical and future drought changes. *Clim. Change* **144**, 535–548 (2017).
25. M. Reichstein, M. Bahn, P. Ciais, D. Frank, M. D. Mahecha, S. I. Seneviratne, J. Zscheischler, C. Beer, N. Buchmann, D. C. Frank, D. Papale, A. Rammig, P. Smith, K. Thonicke, M. van der Velde, S. Vicca, A. Walz, M. Wattenbach, Climate extremes and the carbon cycle. *Nature* **500**, 287–295 (2013).
26. D. Frank, M. Reichstein, M. Bahn, K. Thonicke, D. Frank, M. D. Mahecha, P. Smith, M. van der Velde, S. Vicca, F. Babst, C. Beer, N. Buchmann, J. G. Canadell, P. Ciais, W. Cramer, A. Ibrom, F. Miglietta, B. Poulter, A. Rammig, S. I. Seneviratne, A. Walz, M. Wattenbach, M. A. Zavala, J. Zscheischler, Effects of climate extremes on the terrestrial carbon cycle: Concepts, processes and potential future impacts. *Glob. Chang. Biol.* **21**, 2861–2880 (2015).
27. E. L. Aronson, M. L. Goulden, S. D. Allison, Greenhouse gas fluxes under drought and nitrogen addition in a Southern California grassland. *Soil Biol. Biochem.* **131**, 19–27 (2019).
28. A. Kübert, M. Götz, E. Kuester, A. Piayda, C. Werner, Y. Rothfuss, M. Dubbert, Nitrogen loading enhances stress impact of drought on a semi-natural temperate grassland. *Front. Plant Sci.* **10**, 1051 (2019).
29. L. V. Verchot, E. A. Davidson, H. Cattânio, I. L. Ackerman, H. E. Erickson, M. Keller, Land use change and biogeochemical controls of nitrogen oxide emissions from soils in eastern Amazonia. *Global Biogeochem. Cycles* **13**, 31–46 (1999).
30. E. A. Davidson, F. Y. Ishida, D. C. Nepstad, Effects of an experimental drought on soil emissions of carbon dioxide, methane, nitrous oxide, and nitric oxide in a moist tropical forest. *Glob. Chang. Biol.* **10**, 718–730 (2004).
31. L. Chapuis-Lardy, N. Wrage, A. Metay, J. L. Chotte, M. Bernoux, Soils, a sink for N_2O? A review. *Glob. Change Biol.* **13**, 1–17 (2007).

32. W. Borken, E. Matzner, Reappraisal of drying and wetting effects on C and N mineralization and fluxes in soils. *Glob. Chang. Biol.* **15**, 808–824 (2009).
33. L. Fuchslueger, M. Bahn, K. Fritz, R. Hasibeder, A. Richter, Experimental drought reduces the transfer of recently fixed plant carbon to soil microbes and alters the bacterial community composition in a mountain meadow. *New Phytol.* **201**, 916–927 (2014).
34. X. Xu, Y. Ran, Y. Li, Q. Zhang, Y. Liu, H. Pan, X. Guan, J. Li, J. Shi, L. Dong, Z. Li, H. Di, J. Xu, Warmer and drier conditions alter the nitrifier and denitrifier communities and reduce N_2O emissions in fertilized vegetable soils. *Agric. Ecosyst. Environ.* **231**, 133–142 (2016).
35. P. M. Homyak, S. D. Allison, T. E. Huxman, M. L. Goulden, K. K. Treseder, Effects of drought manipulation on soil nitrogen cycling: A meta-analysis. *J. Geophys. Res. Biogeo.* **122**, 3260–3272 (2017).
36. A. Canarini, F. A. Dijkstra, Dry-rewetting cycles regulate wheat carbon rhizodeposition, stabilization and nitrogen cycling. *Soil Biol. Biochem.* **81**, 195–203 (2015).
37. A. Priemé, S. Christensen, Natural perturbations, drying–wetting and freezing–thawing cycles, and the emission of nitrous oxide, carbon dioxide and methane from farmed organic soils. *Soil Biol. Biochem.* **33**, 2083–2091 (2001).
38. S. D. Goldberg, G. Gebauer, Drought turns a Central European Norway spruce forest soil from an N_2O source to a transient N_2O sink. *Glob. Chang. Biol.* **15**, 850–860 (2009).
39. D.-G. Kim, R. Vargas, B. Bond-Lamberty, M. R. Turetsky, Effects of soil rewetting and thawing on soil gas fluxes: A review of current literature and suggestions for future research. *Biogeosciences* **9**, 2459–2483 (2012).
40. E. Ibraim, B. Wolf, E. Harris, R. Gasche, J. Wei, L. Yu, R. Kiese, S. Eggleston, K. Butterbach-Bahl, M. Zeeman, B. Tuzson, L. Emmenegger, J. Six, S. Henne, J. Mohn, Attribution of N_2O sources in a grassland soil with laser spectroscopy based isotopocule analysis. *Biogeosciences* **16**, 3247–3266 (2019).
41. E. Verhoeven, M. Barthel, L. Yu, L. Celi, D. Said-Pullicino, S. Sleutel, D. Lewicka-Szczebak, J. Six, C. Decock, Early season N_2O emissions under variable water management in rice systems: Source-partitioning emissions using isotope ratios along a depth profile. *Biogeosciences* **16**, 383–408 (2019).
42. E. Harris, A. Joss, L. Emmenegger, M. Kipf, B. Wolf, J. Mohn, P. Wunderlin, Isotopic evidence for nitrous oxide production pathways in a partial nitritation-anammox reactor. *Water Res.* **83**, 258–270

(2015).

43. S. O. Petersen, R. Well, A. Taghizadeh-Toosi, T. J. Clough, Seasonally distinct sources of N_2O in acid organic soil drained for agriculture as revealed by N_2O isotopomer analysis. *Biogeochemistry* **147**, 15–33 (2020).
44. M. Holmstrup, C. Damgaard, I. K. Schmidt, M. F. Arndal, C. Beier, T. N. Mikkelsen, P. Ambus, K. S. Larsen, K. Pilegaard, A. Michelsen, L. C. Andresen, M. Haugwitz, L. Bergmark, A. Priemé, A. S. Zaitsev, S. Georgieva, M. Dam, M. Vestergård, S. Christensen, Long-term and realistic global change manipulations had low impact on diversity of soil biota in temperate heathland. *Sci. Rep.* **7**, 41388 (2017).
45. V. Hammerl, E.-M. Kastl, M. Schloter, S. Kublik, H. Schmidt, G. Welzl, A. Jentsch, C. Beierkuhnlein, S. Gschwendtner, Influence of rewetting on microbial communities involved in nitrification and denitrification in a grassland soil after a prolonged drought period. *Nat. Sci. Rep.* **9**, 2280 (2019).
46. L. Remusat, P.-J. Hatton, P. S. Nico, B. Zeller, M. Kleber, D. Derrien, NanoSIMS study of organic matter associated with soil aggregates: Advantages, limitations, and combination with STXM. *Environ. Sci. Tech.* **46**, 3943–3949 (2012).
47. C. Vogel, C. W. Mueller, C. Höschen, F. Buegger, K. Heister, S. Schulz, M. Schloter, I. Kögel-Knabner, Submicron structures provide preferential spots for carbon and nitrogen sequestration in soils. *Nat. Commun.* **5**, 2947 (2014).
48. K. Li, B. Sinha, P. Hoppe, Speciation of nitrogen-bearing species using negative and positive secondary ion spectra with nano secondary ion mass spectrometry. *Anal. Chem.* **88**, 3281–3288 (2016).
49. A. A. Hartmann, R. L. Barnard, S. Marhan, P. A. Niklaus, Effects of drought and N-fertilization on N cycling in two grassland soils. *Oecologia* **171**, 705–717 (2013).
50. S. Leitner, P. M. Homyak, J. C. Blankinship, J. Eberwein, G. D. Jenerette, S. Zechmeister-Boltenstern, J. P. Schimel, Linking NO and N_2O emission pulses with the mobilization of mineral and organic N upon rewetting dry soils. *Soil Biol. Biochem.* **115**, 461–466 (2017).
51. IPCC, *2006 IPCC Guidelines for National Greenhouse Gas Inventories* (IGES, 2006).
52. R. Well, H. Flessa, L. Xing, J. Xiaotang, V. Römheld, Isotopologue ratios of N_2O emitted from microcosms with NH_4^+ fertilized arable soils under conditions favoring nitrification. *Soil Biol. Biochem.* **40**, 2416–2426 (2008).

53. A. Castellano-Hinojosa, J. González-López, E. J. Bedmar, Distinct effect of nitrogen fertilisation and soil depth on nitrous oxide emissions and nitrifiers and denitrifiers abundance. *Biol. Fertil. Soils* **54**, 829–840 (2018).
54. J. P. Schimel, Life in dry soils: Effects of drought on soil microbial communities and processes. *Annu. Rev. Ecol. Evol. Syst.* **49**, 409–432 (2018).
55. K. A. Thorn, M. A. Mikita, Nitrite fixation by humic substances nitrogen-15 nuclear magnetic resonance evidence for potential intermediates in chemodenitrification. *Soil Sci. Soc. Am. J.* **64**, 568–582 (2000).
56. B.-R. Lee, R. Zaman, J.-C. Avice, A. Ourry, T.-H. Kim, Sulfur use efficiency is a significant determinant of drought stress tolerance in relation to photosynthetic activity in *Brassica napus* cultivars. *Front. Plant Sci.* **7**, 459 (2016).
57. G. J. Burch, I. D. Moore, J. Burns, Soil hydrophobic effects on infiltration and catchment runoff. *Hydrol. Process.* **3**, 211–222 (1989).
58. A. Sowerby, B. A. Emmett, A. Tietema, C. Beier, Contrasting effects of repeated summer drought on soil carbon efflux in hydric and mesic heathland soils. *Glob. Chang. Biol.* **14**, 2388–2404 (2008).
59. L. Yu, E. Harris, D. Lewicka-Szczebak, J. Mohn, What can we learn from N_2O isotope data? - Analytics, processes and modelling. *Rapid Commun. Mass Spectrom.* **34**, e8858 (2020).
60. J. Wei, E. Ibraim, N. Brüggemann, H. Vereecken, J. Mohn, First real-time isotopic characterisation of N_2O from chemodenitrification. *Geochim. Cosmochim. Acta* **267**, 17–32 (2019).
61. J. Kreyling, A. H. Schweiger, M. Bahn, P. Ineson, M. Migliavacca, T. Morel-Journel, J. R. Christiansen, N. Schtickzelle, K. S. Larsen, To replicate, or not to replicate—That is the question: How to tackle nonlinear responses in ecological experiments. *Ecol. Lett.* **21**, 1629–1638 (2018).
62. H. F. Birch, Mineralization of plant nitrogen following alternate wet and dry conditions. *Plant Soil* **20**, 43–49 (1964).
63. J. Ingrisch, S. Karlowsky, A. Anadon-Rosell, R. Hasibeder, A. König, A. Augusti, G. Gleixner, M. Bahn, Land use alters the drought responses of productivity and CO_2 fluxes in mountain grassland. *Ecosystems* **21**, 689–703 (2018).
64. R. T. Venterea, Nitrite-driven nitrous oxide production under aerobic soil conditions: Kinetics and biochemical controls. *Glob. Chang. Biol.* **13**, 1798–1809 (2007).
65. J. Wei, W. Amelung, E. Lehndorff, M. Schloter, H. Vereecken, N. Brüggemann, N_2O and NO_x emissions by reactions of nitrite with soil organic matter of a Norway spruce forest. *Biogeochemistry*

132, 325–342 (2017).

66. M. Prokopiou, P. Martinerie, C. J. Sapart, E. Witrant, G. Monteil, K. Ishijima, S. Bernard, J. Kaiser, I. Levin, T. Blunier, D. Etheridge, E. Dlugokencky, R. S. W. van de Wal, T. Röckmann, Constraining N_2O emissions since 1940 using firn air isotope measurements in both hemispheres. *Atmos. Chem. Phys.* **17**, 4539–4564 (2017).
67. J. W. Erisman, M. A. Sutton, J. Galloway, Z. Klimont, W. Winiwarter, How a century of ammonia synthesis changed the world. *Nat. Geosci.* **1**, 636–639 (2008).
68. A. E. Davidson, P. A. Matson, P. M. Vitousek, R. Riley, K. Dunkin, C. Garcia-Mendez, J. M. Maass, Processes regulating soil emissions of NO and N^2O in a seasonally dry tropical forest. *Ecology* **74**, 130–139 (1993).
69. R. Ruser, H. Flessa, R. Russow, G. Schmidt, F. Buegger, J. C. Munch, Emission of N_2O, N_2 and CO_2 from soil fertilized with nitrate: Effect of compaction, soil moisture and rewetting. *Soil Biol. Biochem.* **38**, 263–274 (2006).
70. E. Harris, T. Ladreiter-Knauss, K. Butterbach-Bahl, B. Wolf, M. Bahn, Land-use and abandonment alters methane and nitrous oxide fluxes in mountain grasslands. *Sci. Total Environ.* **628-629**, 997–1008 (2018).
71. M. Bahn, M. Schmitt, R. Siegwolf, A. Richter, N. Brüggemann, Does photosynthesis affect grassland soil-respired CO_2 and its carbon isotope composition on a diurnal timescale? *New Phytol.* **182**, 451–460 (2009).
72. S. Meyer, J. Leifeld, M. Bahn, J. Fuhrer, Land-use change in subalpine grassland soils: Effect on particulate organic carbon fractions and aggregation. *J. Plant Nutr. Soil Sci.* **175**, 401–409 (2012).
73. L. Fuchslueger, E.-M. Kastl, F. Bauer, S. Kienzl, R. Hasibeder, T. Ladreiter-Knauss, M. Schmitt, M. Bahn, M. Schloter, A. Richter, U. Szukics, Effects of drought on nitrogen turnover and abundances of ammonia-oxidizers in mountain grassland. *Biogeosciences* **11**, 6003–6015 (2014).
74. H. J. De Boeck, S. Bassin, M. Verlinden, M. Zeiter, E. Hiltbrunner, Simulated heat waves affected alpine grassland only in combination with drought. *New Phytol.* **209**, 531–541 (2015).
75. H. J. De Boeck, E. Hiltbrunner, M. Verlinden, S. Bassin, M. Zeiter, Legacy effects of climate extremes in alpine grassland. *Front. Plant Sci.* **9**, 1586 (2018).
76. L. Fuchslueger, B. Wild, M. Mooshammer, M. Takriti, S. Kienzl, A. Knoltsch, F. Hofhansl, M. Bahn, A. Richter, Microbial carbon and nitrogen cycling responses to drought and temperature in differently managed mountain grasslands. *Soil Biol. Biochem.* **135**, 144–153 (2019).

77. I. J. Slette, A. K. Post, M. Awad, T. Even, A. Punzalan, S. Williams, M. D. Smith, A. K. Knapp, How ecologists define drought, and why we should do better. *Glob. Chang. Biol.* **25**, 3193–3200 (2019).
78. S. Toyoda, N. Kuroki, N. Yoshida, K. Ishijima, Y. Tohjima, T. Machida, Decadal time series of tropospheric abundance of N2O isotopomers and isotopologues in the northern hemisphere obtained by the long-term observation at Hateruma Island, Japan. *J. Geophys. Res. Atmos.* **118**, 3369–3381 (2013).
79. N. Pirk, M. Mastepanov, F.-J. Parmentier, M. Lund, P. Crill, T. R. Christensen, Calculations of automatic chamber flux measurements of methane and carbon dioxide using short time series of concentrations. *Biogeosciences* **13**, 903–912 (2016).
80. C. D. Keeling, The concentration and isotopic abundances of atmospheric carbon dioxide in rural areas. *Geochim. Cosmochim. Acta* **13**, 322–334 (1958).
81. C. D. Keeling, The concentration and isotopic abundances of carbon dioxide in rural and marine air. *Tellus* **24**, 277–298 (1960).
82. J. Mohn, W. Gutjahr, S. Toyoda, E. Harris, E. Ibraim, H. Geilmann, P. Schleppi, T. Kuhn, M. F. Lehmann, C. Decock, R. A. Werner, N. Yoshida, W. A. Brand, Reassessment of the NH_4NO_3thermal decomposition technique for calibration of the N_2O isotopic composition. *Rapid Commun. Mass Spectrom.* **30** (2016).
83. J. Mohn, B. Tuzson, A. Manninen, N. Yoshida, S. Toyoda, W. A. Brand, L. Emmenegger, Site selective real-time measurements of atmospheric N_2O isotopomers by laser spectroscopy. *Atmos. Meas. Tech.* **5**, 1601–1609 (2012).
84. E. Harris, D. D. Nelson, W. Olszewski, M. Zahniser, K. E. Potter, B. J. McManus, A. Whitehill, R. G. Prinn, S. Ono, Development of a spectroscopic technique for continuous online monitoring of oxygen and site-specific nitrogen isotopic composition of atmospheric nitrous oxide. *Anal. Chem.* **86**, 1726–1734 (2014).
85. E. Harris, S. Henne, C. Hüglin, C. Zellweger, B. Tuzson, E. Ibraim, L. Emmenegger, J. Mohn, Tracking nitrous oxide emission processes at a suburban site with semicontinuous, in situ measurements of isotopic composition. *J. Geophys. Res. Atmos.* **122**, 1850–1870 (2017).
86. T. R. A. Denk, J. Mohn, C. Decock, D. Lewicka-Szczebak, E. Harris, K. Butterbach-Bahl, R. Kiese, B. Wolf, The nitrogen cycle: A review of isotope effects and isotope modeling approaches. *Soil Biol. Biochem.* **105**, 121–137 (2017).

87. B. Wolf, L. Merbold, C. Decock, B. Tuzson, E. Harris, J. Six, L. Emmenegger, J. Mohn, First on-line isotopic characterization of N_2O emitted from intensively managed grassland. *Biogeosciences* **12**, 2517–2531 (2015).
88. D. Wu, J. R. Köster, L. M. Cárdenas, N. Brüggemann, D. Lewicka-Szczebak, R. Bol, N2O source partitioning in soils using ^{15}N site preference values corrected for the N_2O reduction effect. *Rapid Commun. Mass Spectrom.* **30**, 620–626 (2016).
89. N. E. Ostrom, A. Pitt, R. Sutka, P. H. Ostrom, A. S. Grandy, K. M. Huizinga, G. P. Robertson, Isotopologue effects during N_2O reduction in soils and in pure cultures of denitrifiers. *J. Geophys. Res. Biogeosci.* **112**, G02005 (2007).
90. P. Lachouani, A. Frank, W. Wanek, A suite of sensitive chemical methods to determine the $\delta^{15}N$ of ammonium, nitrate and total dissolved N in soil extracts. *Rapid Commun. Mass Spectrom.* **24**, 3615–3623 (2010).
91. R. Hood-Nowotny, N. H.-N. Umana, E. Inselbacher, P. Oswald-Lachouani, W. Wanek, Alternative methods for measuring inorganic, organic, and total dissolved nitrogen in soil. *Soil Sci. Soc. Am. J.* **74**, 1018–1027 (2010).
92. T. Lueders, M. Manefield, M. W. Friedrich, Enhanced sensitivity of DNA- and rRNA-based stable isotope probing by fractionation and quantitative analysis of isopycnic centrifugation gradients. *Environ. Microbiol.* **6**, 73–78 (2004).
93. S. Töwe, S. Wallisch, A. Bannert, D. Fischer, B. Hai, F. Haesler, K. Kleineidam, M. Schloter, Improved protocol for the simultaneous extraction and column-based separation of DNA and RNA from different soils. *J. Microbiol. Methods* **84**, 406–412 (2011).
94. S. Töwe, A. Albert, K. Kleineidam, R. Brankatschk, A. Dümig, G. Welzl, J. C. Munch, J. Zeyer, M. Schloter, Abundance of microbes involved in nitrogen transformation in the rhizosphere of *Leucanthemopsis alpina* (L.) heywood grown in soils from different sites of the Damma glacier forefield. *Microb. Ecol.* **60**, 762–770 (2010).
95. S. Geschwendtner, J. Esperschütz, F. Buegger, M. Reichmann, M. Müller, J. C. Munch, M. Schloter, Effects of genetically modified starch metabolism in potato plants on photosynthate fluxes into the rhizosphere and on microbial degraders of root exudates. *FEMS Microbiol. Ecol.* **76**, 564–575 (2011).
96. C. W. Mueller, A. Kölbl, C. Hoeschen, F. Hillion, K. Heister, A. M. Herrmann, I. Kögel-Knabner, Submicron scale imaging of soil organic matter dynamics using NanoSIMS—From single particles

to intact aggregates. *Org. Geochem.* **42**, 1476–1488 (2012).

97. V. Amrhein, S. Greenland, B. McShane, Scientists rise up against statistical significance. *Nature* **567**, 305–307 (2019).
98. R Core Team, *R: A Language and Environment for Statistical Computing* (R Foundation for Statistical Computing, 2017).
99. C. Arias-Navarro, E. Díaz-Pinés, S. Klatt, P. Brandt, M. C. Rufino, K. Butterbach-Bahl, L. V. Verchot, Spatial variability of soil N_2O and CO_2 fluxes in different topographic positions in a tropical montane forest in Kenya. *J. Geophys. Res. Biogeo.* **122**, 514–527 (2017).
100. D. A. Turner, D. Chen, I. E. Galbally, R. Leuning, R. B. Edis, Y. Li, K. Kelly, F. Phillips, Spatial variability of nitrous oxide emissions from an Australian irrigated dairy pasture. *Plant Soil* **309**, 77–88 (2008).
101. R. G. Prinn, R. F. Weiss, P. J. Fraser, P. G. Simmonds, D. M. Cunnold, F. N. Alyea, S. O'Doherty, P. Salameh, B. R. Miller, J. Huang, R. H. J. Wang, D. E. Hartley, C. Harth, L. P. Steele, G. Sturrock, P. M. Midgley, A. McCulloch, A history of chemically and radiatively important gases in air deduced from ALE/GAGE/AGAGE. *J. Geophys. Res. Atmos.* **105**, 17751–17792 (2000).
102. R. G. Prinn, R. F. Weiss, P. J. Fraser, P. G. Simmonds, D. M. Cunnold, S. J. O'Doherty, P. K. Salameh, L. W. Porter, P. B. Krummel, R. H. J. Wang, B. R. Miller, C. Harth, B. R. Greally, V. Woy, F.A., L. P. Steele, J. Mühle, W. T. Sturges, F. N. Alyea, J. Huang, D. E. Hartley, *The ALE/GAGE AGAGE Network* (2013); doi: 10.3334/CDIAC/atg.db1001.
103. R. L. Sutka, N. E. Ostrom, P. H. Ostrom, H. Gandhi, J. A. Breznak, Erratum: Nitrogen isotopomer site preference of N_2O produced by *Nitrosomonas europaea* and *Methylococcus capsulatus* Bath. *Rapid Commun. Mass Spectrom.* **18**, 1411–1412 (2004).
104. R. L. Sutka, N. E. Ostrom, P. H. Ostrom, J. A. Breznak, H. Gandhi, A. J. Pitt, F. Li, Distinguishing nitrous oxide production from nitrification and denitrification on the basis of isotopomer abundances. *Appl. Environ. Microbiol.* **72**, 638–644 (2006).
105. S. Toyoda, H. Mutobe, H. Yamagishi, N. Yoshida, Y. Tanji, Fractionation of N_2O isotopomers during production by denitrifier. *Soil Biol. Biochem.* **37**, 1535–1545 (2005).
106. S. Toyoda, M. Yano, S.-i. Nishimura, H. Akiyama, A. Hayakawa, K. Koba, S. Sudo, K. Yagi, A. Makabe, Y. Tobari, N. O. Ogawa, N. Ohkouchi, K. Yamada, N. Yoshida, Characterization and production and consumption processes of N_2O emitted from temperate agricultural soils determined via isotopomer ratio analysis. *Global Biogeochem. Cycles* **25**, GB2008 (2011).

107. P. Wunderlin, M. F. Lehmann, H. Siegrist, B. Tuzson, A. Joss, L. Emmenegger, J. Mohn, Isotope signatures of N_2O in a mixed microbial population system: Constraints on N_2O producing pathways in wastewater treatment. *Environ. Sci. Technol.* **47**, 1339–1348 (2013).

108. J. Heil, B. Wolf, N. Brüggemann, L. Emmenegger, B. Tuzson, H. Vereecken, J. Mohn, Site-specific ^{15}N signatures of abiotically-produced N_2O. *Geochim. Cosmochim. Acta* **139**, 72–82 (2014).

109. A. Schilt, E. J. Brook, T. K. Bauska, D. Baggenstos, H. Fischer, F. Joos, V. V. Petrenko, H. Schaefer, J. Schmitt, J. P. Severinghaus, R. Spahni, T. F. Stocker, Isotopic constraints on marine and terrestrial N_2O emissions during the last deglaciation. *Nature* **516**, 234–237 (2014).

110. J. Mohn, B. Wolf, S. Toyoda, C.-T. Lin, M.-C. Liang, N. Brüggemann, H. Wissel, A. E. Steiker, J. Dyckmans, L. Szwec, N. E. Ostrom, K. L. Casciotti, M. Forbes, A. Giesemann, R. Well, R. R. Doucett, C. T. Yarnes, A. R. Ridley, J. Kaiser, N. Yoshida, Interlaboratory assessment of nitrous oxide isotopomer analysis by isotope ratio mass spectrometry and laser spectroscopy: Current status and perspectives. *Rapid Commun. Mass Spectrom.* **28**, 1995–2007 (2014).